

Polymer Chemistry

rsc.li/polymers



ISSN 1759-9962

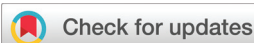


ROYAL SOCIETY
OF CHEMISTRY

PAPER

Zhi-Gang Zheng, Weian Zhang *et al.*

Synthesis of POSS-functionalized liquid crystalline block copolymers via RAFT polymerization for stabilizing blue phase helical soft superstructures



Cite this: *Polym. Chem.*, 2018, **9**, 2101

Synthesis of POSS-functionalized liquid crystalline block copolymers *via* RAFT polymerization for stabilizing blue phase helical soft superstructures†

Jianqiu Jin,^{‡a} Mingjie Tang,^{‡a} Zhenghe Zhang,^a Kang Zhou,^a Yun Gao,^a Zhi-Gang Zheng^{ID} ^{*a,b} and Weian Zhang^{ID} ^{*a}

A series of POSS-functionalized liquid crystalline block copolymers (LC BCPs), PHEMAPOSS-*b*-P6CBMA, containing a crystalline polyhedral oligomeric silsesquioxane (POSS) block and a mesogenic cyanobiphenyl block, were prepared *via* reversible addition–fragmentation transfer (RAFT) polymerization for the first time and utilized to stabilize blue phase (BP) liquid crystals through facile doping. Using the advantages of both the POSS and polymer, a new strategy, which is distinct from the commonly adopted strategy for polymer stabilization of the BP, has been established. This new BP system with a wide BP range covering the typical room temperature range (*i.e.* 25–30 °C) leaps over intricate processing barriers, which are inevitable in conventional photo-induced polymer stabilization. In particular, improved electro-optical (E-O) properties of the BP, including lower driving voltage, lower hysteresis and a higher Kerr constant (*K*) compared with the common BP stabilized *via* photopolymerization, were obtained by optimizing the concentration of the doped LC BCP. Differential scanning calorimetry (DSC) and thermogravimetric analysis (TGA) were employed to evaluate the thermal properties of the LC BCPs, and the results indicated that the introduction of POSS enhanced the thermostabilities of the copolymers effectively. Such an ingenious strategy provides a brilliant and easy way to form large size BP displays and other devices that are incompatible with UV light exposure during the working process.

Received 25th January 2018,
Accepted 9th March 2018

DOI: 10.1039/c8py00136g

rsc.li/polymers

Introduction

Polyhedral oligomeric silsesquioxane (POSS) is attractive as one of the promising candidates for constructing inorganic–organic hybrid materials because of its well-defined cube-like structure with an inorganic silica core surrounded by eight functional organic corner groups.^{1–5} In recent years, with the rapid development of living/controlled polymerization techniques in polymer science, many novel POSS-containing hybrid polymers with well-defined topological structures have been developed,⁶ including star-shaped,^{7–11} telechelic,^{12–17} dendrimers,^{18–20} alternating copolymers,^{21–23} and block copolymers (BCPs).^{24–27} Among hybrid polymers, BCPs in particu-

lar, which exhibit microphase-separated structures due to the nature of POSS and possess advantageous properties, have attracted much interest.^{28–30} Hayakawa *et al.* reported the synthesis of a POSS-containing block copolymer of poly (POSS methacrylate-*block*-2,2,2-trifluoroethyl methacrylate) (PMAPOSS-*b*-PTFEMA) with a precisely controlled structure *via* reversible addition–fragmentation transfer (RAFT) polymerization, and this polymer could self-assemble into fancy perpendicularly oriented nanodomains.³¹

Monomers bearing mesogenic moieties are popular as some of the useful candidates for constructing BCP-based materials, *i.e.* liquid crystalline block copolymers (LC BCPs), because of the functionality of the LC block.^{32–42} As a result, both the microphase separation properties of BCPs and the self-organizing behaviors of liquid crystal (LC) polymers are integrated into one polymer system.⁴³ Recently, some well-designed LC BCPs have been constructed to endow advanced materials with potential electronic, photonic, or photoresponsive functionalities.^{34,44,45}

The blue phase (BP), a specific LC phase in a system with high chirality, generally exists between the isotropic and chiral nematic (N*) phases, giving rise to a fascinating soft material with a self-assembled 3D cubic helical soft superstructure

^aShanghai Key Laboratory of Functional Materials Chemistry, Department of Physics, East China University of Science and Technology, 130 Meilong Road, Shanghai 200237, China. E-mail: wazhang@ecust.edu.cn, zgzheng@ecust.edu.cn;

Fax: +86-21-64253033; Tel: +86-21-64253033

^bState Key Laboratory of Applied Optics, Changchun Institute of Optics, Fine Mechanics and Physics, Chinese Academy of Sciences, Changchun, 130033, China

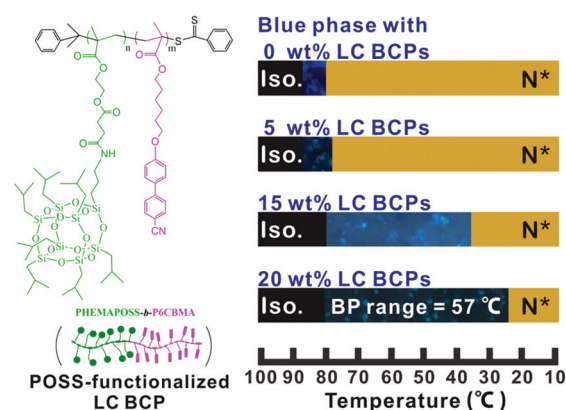
†Electronic supplementary information (ESI) available: Experimental details and additional data. See DOI: 10.1039/c8py00136g

‡These authors contributed equally to this work.

formed by double twisted cylinders (DTCs) under certain circumstances.^{46,47} The lattice constant of the BP is comparable to the scale of the wavelength of light, thereby endowing such a phase with selective light reflection, presenting significant colorful platelets that are the typical optical texture of a BP. Such an arrangement possesses a fast response on the scale of submilliseconds driven by an electric field due to the short coherent length, therefore enabling versatile advanced electro-optical (E-O) applications.^{47,48} The major problem that hinders the substantial applications of BP materials is their weak structural thermostability (*i.e.* a narrow temperature range of 2–3 K), which has motivated abundant endeavours with the aim of resolving this issue and improving the performance of BP materials.^{49–57} In particular, polymer stabilized BP (PSBP) materials, which were first proposed by Kikuchi *et al.* in 2002,⁵⁸ have been widely used in the fields of science and engineering, such as in displays and photonics.^{59,60} However, some bottlenecks of PSBP materials, such as high driving voltage, and voltage-induced hysteresis due to the increasing number of monomers, still have not been overcome. Furthermore, the preparation of PSBP materials is intricate and requires elaborate techniques, including complex processes, precise temperature control and uniform ultraviolet (UV) light intensity, all of which are great challenges to the application and engineering of BP materials.

In the past few decades, POSS, as an interesting nanosized inorganic–organic hybrid molecule with the superior characteristics of low surface energy and unique structure, has been loaded in some LC media. Jeong *et al.* employed POSS for the vertical alignment (VA) of liquid crystals and Jung *et al.* proposed that POSS can optimize the E-O performance of liquid crystal systems.^{61,62} Kemiklioglu *et al.* observed a significant reduction of the driving voltage of PSBP materials based on acrylated POSS monomers, however, the complicated preparation processes and high technological conditions that are necessary for conventional adopted polymer stabilization are inevitable.⁶³

Herein, we designed and synthesized a POSS-functionalized LC BCP (HEMAPOSS-*b*-P6CBMA) *via* RAFT polymerization using monomers of POSS and mesogenic cyanobiphenyl, both of which possess a long spacer to overcome the polymerization barrier as well as enhance the molecular flexibility (Scheme 1). Such a judiciously designed LC BCP exhibits improved miscibility even when the concentration reaches 20 wt% in the BP medium due to the mesogens embedded into the LC host. This is difficult to achieve with common POSS-functionalized BCPs to the best of our knowledge. A relatively stable BP, with a wide BP range covering the typical room temperature range (*i.e.* 25–30 °C), was obtained through facile doping of the LC BCP (HEMAPOSS₄₀-*b*-P6CBMA₁₆₇), while leaping over the aforementioned processing barriers that are regarded as inevitable in conventional photo-induced polymer stabilization. Moreover, the E-O properties of the doped BPs, including the driving voltage, hysteresis and Kerr effect, displayed significant improvements compared with the conventional PSBP samples. Such an approach to stabilizing BP materials by directly



Scheme 1 The structure of the POSS-functionalized LC BCP and the phase transition behavior of the blue phase liquid crystal containing different amounts of the POSS-functionalized LC BCP.

mixing an elaborately synthesized POSS-functionalized LC BCP is distinct from polymer stabilization methods as well as other approaches that have been commonly used to enhance the BP arrangement, and produces another stable BP material candidate, which might be more appropriate for large size BP displays and other devices that are incompatible with UV light exposure during the working process, such as micro-phonic devices used in biomedicine for protein detection *in vivo*.

Experimental section

Materials

The POSS-functionalized monomer (HEMAPOSS) and RAFT agent cumyl dithiobenzoate (CDB) were prepared according to our previous work,⁶⁴ and the synthetic route to prepare HEMAPOSS is shown in Scheme S1.† 2,2'-Azobisisobutyronitrile (AIBN) was recrystallized three times from ethanol. Dichloromethane (DCM), triethylamine (TEA) and tetrahydrofuran (THF) were dried over sodium and distilled before use. Methacryloyl chloride (95%, Aladdin), 2-hydroxyethylmethacrylate (HEMA, 96%, Aladdin), 4-cyano-4'-hydroxybiphenyl (99%, Aladdin), succinic anhydride (98%, Aladdin), 6-chloro-1-hexanol (95%, Aladdin), nematic liquid crystals (NLCs) SLC-1717 (supplied by Slichem Co. Ltd), chiral dopant R5011 (from Jiangsu Hecheng Advanced Materials Co. Ltd), and other reagents were used directly as received.

Characterization

The ¹H NMR measurement was performed using a BRUKER AV400 spectrophotometer using tetramethylsilane (TMS) as the internal reference and CDCl₃ as the solvent. The number average weight (M_n) and polydispersity index (M_w/M_n) were determined using a Waters 1515 size exclusion chromatography (SEC) system with THF as the eluent at a 1 mL min⁻¹ flow rate and polystyrene as the standard.

The thermostability of the sample was measured using a PerkinElmer Pyris 1 Thermal Gravimetric Analyzer (TGA)

under nitrogen and air, separately. The sample (flow rate: 60 mL min⁻¹) was heated up from 0 to 800 °C at the heating rate of 10 °C min⁻¹.

Differential scanning calorimetry (DSC) was carried out using a PerkinElmer Diamond DSC instrument under nitrogen. The samples were first heated up to 200 °C and held at this temperature for 10 min, then the sample was cooled to -50 °C. The second heating scan was performed from -50 to 200 °C at a rate of 10 °C min⁻¹ and all the thermograms were recorded.

Synthesis of the POSS-functionalized homopolymer (PHEMAPOSS)

PHEMAPOSS was prepared *via* RAFT polymerization of the POSS-functionalized monomer HEMAPOSS using CDB as the RAFT agent, according to our previous work.⁶⁴

Synthesis of the LC BCP (PHEMAPOSS-*b*-P6CBMA)

In a typical process, PHEMAPOSS (0.3 g, 0.0061 mmol), 6CBMA (1.2 g, 3.3 mmol) and AIBN (42 μL, 5 mg mL⁻¹ AIBN THF solution, 0.0012 mmol) were dissolved in 4 mL THF and placed in a glass tube with a magnetic stirring bar. The mixture was degassed *via* four freeze-pump-thaw cycles. The polymerization was performed in an oil bath at 70 °C for 12 h after the tube was sealed under vacuum. The reaction was quenched using liquid nitrogen. Finally, the mixture was precipitated into methanol five times, and the product was dried under vacuum at 50 °C for 24 h to obtain PHEMAPOSS-*b*-P6CBMA.

Sample preparation and measurement

The POSS-functionalized LC BCP (*i.e.* PHEMAPOSS₄₀-*b*-P6CBMA₁₆₇) was mixed into a blue phase liquid crystal (BPLC) host with additional solvent, dichloromethane, to enable a better dispersion of the polymer in the solution, then this was stirred at room temperature for at least 1 hour and heated to 50 °C for another 30 min to remove the solvent through evaporation (Scheme S3†). The BPLC host was prepared by mixing a commercial NLC, SLC-1717, and a commonly used chiral agent, R5011 (supported by Merck Serono Co., Ltd.), in a weight ratio of 95.2:4.8. Four samples containing 5 wt%, 15 wt%, 20 wt% and 25 wt% of the LC BCP were prepared. The sample was confined in a 9.5 μm-thick in-plane-switching (IPS) LC cell with interdigital stripe indium tin oxide (ITO) electrodes on a single substrate (width of the electrode: 12 μm, gap between the adjacent electrodes: 12 μm) and settled on a precisely controlled hot stage (LTS120E, Linkam). The phase transition behavior was observed using a polarized optical microscope (POM, Nikon LVPOL 100) with a crossed polarizer in reflection mode during sample cooling with a rate of 0.5 °C min⁻¹. The BP texture was observed using a charge-coupled device (CCD, Nikon, DS-U3) fixed on the POM and the corresponding reflection spectrum was detected using a fiber connected spectrometer (Avantes USB2048).

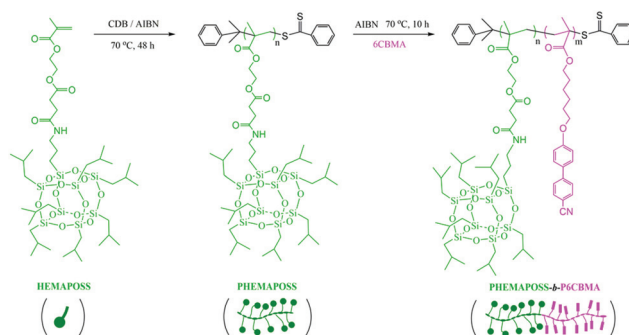
A 1 kHz square-wave alternating current (AC) electric-signal was applied on the cell, while a 532 nm double-frequency neo-

dymium-doped yttrium aluminium garnet (Nd:YAG) laser, with a polarization direction of ±45° with respect to the electrode orientation, moved along the cell normal as the probe light to ensure the highest possible refractive index modulation when applying a voltage. Thus, the voltage-*versus*-transmittance (VT) curve was tested. The response time of the sample was tested by recording the transmission intensity changes in alternate OFF (*i.e.* removing voltage) and ON (*i.e.* applying a saturation voltage) states using a photoelectric converter connected to the oscilloscope. The Kerr constant (*K*) was determined by fitting the curve of the electric-field dependent birefringence using the extended Kerr theory,⁶⁵ while the birefringence of the sample was tested using the commonly used Senarmont method. Herein, the voltage dependent capacitance was tested using a capacitance meter (Hioki Hitester 3532-50) to obtain the dielectric constant of the LC host.

Results and discussion

Synthesis of LC BCP PHEMAPOSS-*b*-P6CBMA

A series of POSS-functionalized LC BCPs, PHEMAPOSS-*b*-P6CBMA, were synthesized *via* RAFT polymerization, and the synthetic route is illustrated in Scheme 2. Firstly, the HEMAPOSS monomer (Scheme S1†) and PHEMAPOSS homopolymer were prepared, separately. Here, our group designed and synthesized a novel POSS monomer (HEMAPOSS) with a long spacer between the POSS unit and the methacrylate group before it, which decreases the steric effects of the large cube-like POSS units in the free-radical polymerization. The POSS-functionalized homopolymers (PHEMAPOSS) with a higher degree of polymerization (DP) were successfully obtained *via* RAFT polymerization. The polymerization was carried out in THF at 70 °C for 24 h using AIBN as an initiator and CDB as a RAFT agent. The molar ratio between HEMAPOSS, AIBN and CDB was fixed to 50/0.3/1. The SEC trace (Fig. 1, trace 5) without a shoulder and with only a tiny tail at a low elution volume demonstrated that the RAFT polymerization of the POSS-containing monomer HEMAPOSS had been achieved. The ¹H NMR spectrum (Fig. S4†) was also measured to characterize the PHEMAPOSS homopolymer, and the number molecular weight (*M*_n, NMR, PHEMAPOSS) was calculated using the



Scheme 2 Synthetic procedure for PHEMAPOSS-*b*-P6CBMA.

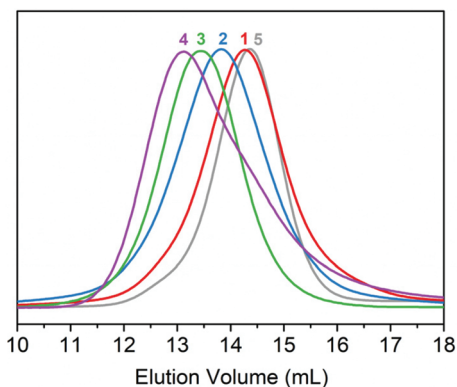


Fig. 1 The SEC curves of (1) PHEMAPOSS₄₀-*b*-P6CBMA₃₂, (2) PHEMAPOSS₄₀-*b*-P6CBMA₈₉, (3) PHEMAPOSS₄₀-*b*-P6CBMA₁₆₇, (4) PHEMAPOSS₄₀-*b*-P6CBMA₂₉₀ and (5) PHEMAPOSS₄₀.

formula $M_{n, \text{NMR, PHEMAPOSS}} = [M]_0/[CTA]_0 \times M_{\text{HEMAPOSS}} \times \chi + M_{\text{CDB}}$, where M_{HEMAPOSS} , M_{CDB} and χ are the molecular weight of HEMAPOSS, molecular weight of CDB and monomer conversion, respectively. The results showed that the DP_{HEMAPOSS} and $M_{n, \text{NMR, PHEMAPOSS}}$ of the homopolymer PHEMAPOSS were 40 and 43 400 g mol⁻¹, respectively.

After the synthesis of the LC monomer 6CBMA (Scheme S2 and Fig. S3†), the PHEMAPOSS homopolymer was used as a macro chain transfer agent (CTA) to synthesize the LC BCPs PHEMAPOSS-*b*-P6CBMA. The polymerization was carried out in THF at 70 °C. Four block copolymers with the same PHEMAPOSS block length and different P6CBMA block lengths were obtained, and the polymerization results are listed in Table 1. The SEC curves of the PHEMAPOSS-*b*-P6CBMA block copolymers are shown in Fig. 1. It can be clearly observed that the peaks of the SEC curves shifted to lower elution volumes with increasing P6CBMA block length. Additionally, the polymerization of the P6CBMA block led to a substantial increase of the PDI (Table 1), which is probably due to the non-negligible presence of dead chains in the macro CTA. The ¹H NMR spectrum of the PHEMAPOSS-*b*-P6CBMA block copolymer is shown in Fig. 2. By comparing the integration area of the signal at 6.92 ppm (c, aromatic proton from the biphenyl unit), to that of the signal at

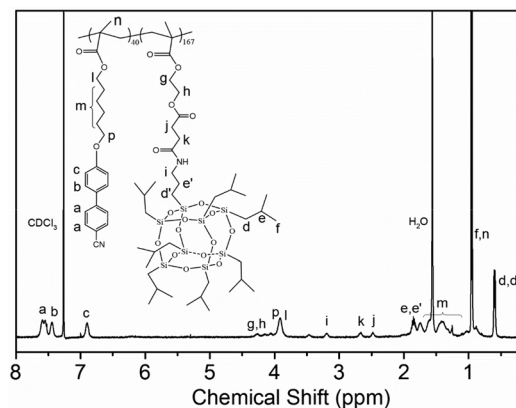


Fig. 2 ¹H NMR spectrum of PHEMAPOSS₄₀-*b*-P6CBMA₁₆₇ in CDCl₃.

0.53 ppm (d, d', -Si-CH₂-), the DP_{P6CBMA} in the P6CBMA block was determined as $DP_{\text{P6CBMA}} = (16 \times I_{2.22}) / (2 \times I_{0.53}) \times DP_{\text{HEMAPOSS}}$, and the $M_{n, \text{NMR, PHEMAPOSS-}b\text{-P6CBMA}}$ of the PHEMAPOSS-*b*-P6CBMA block copolymers was determined as $M_{n, \text{NMR, PHEMAPOSS-}b\text{-P6CBMA}} = M_{n, \text{NMR, PHEMAPOSS}} + DP_{\text{P6CBMA}} \times M_{n, \text{6CBMA}}$, where $M_{n, \text{6CBMA}}$ is the molecular weight of the 6CBMA monomer.

Thermal properties of the LC BCPs

DSC measurements were performed to identify the thermal transitions of PHEMAPOSS-*b*-P6CBMA. Firstly, all the samples were heated up to 200 °C and held at this temperature for 10 min to remove their thermal history. After the cooling process, all of their second heating traces were recorded and are shown in Fig. 3. We can clearly see that the clearing point (T_i) of the LC BCPs at around 150 °C rises with the increase of POSS content. This result implies that the steric POSS unit in the LC BCP may render the movement of the whole block copolymer more difficult, leading to a higher temperature being required to achieve the isotropic transition. Additionally, the glass-transition temperature (T_g) could only be observed clearly from the curve of PHEMAPOSS₄₀-*b*-P6CBMA₂₉₀ at

Table 1 The results of the LC BCPs obtained via RAFT polymerization

Polymers	$M_{n, \text{SEC}}^a$	$M_{n, \text{NMR}}^b$	PDI ^a	wt% (P6CBMA)
PHEMAPOSS ₄₀	21 000	43 400	1.15	0
PHEMAPOSS ₄₀ - <i>b</i> -P6CBMA ₃₂	23 100	55 100	1.30	21
PHEMAPOSS ₄₀ - <i>b</i> -P6CBMA ₈₉	29 700	75 700	1.32	43
PHEMAPOSS ₄₀ - <i>b</i> -P6CBMA ₁₆₇	40 500	104 100	1.27	58
PHEMAPOSS ₄₀ - <i>b</i> -P6CBMA ₂₉₀	51 400	148 700	1.31	70

^a Molecular weights ($M_{n, \text{SEC}}$) and molecular weight distributions (PDI) were evaluated using SEC with polystyrene standards. ^b The final composition of the block copolymer and $M_{n, \text{NMR}}$ were determined from the integration of the ¹H NMR spectra.

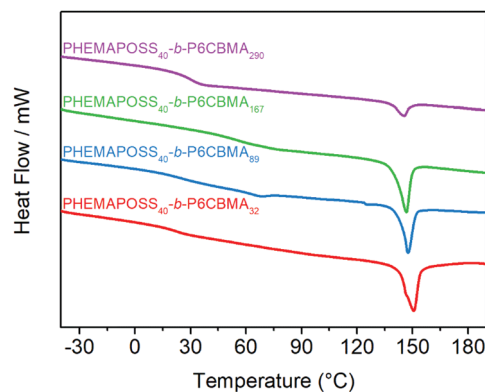


Fig. 3 DSC curves of PHEMAPOSS-*b*-P6CBMA on second heating processes with a heating rate of 10 °C min⁻¹ under a nitrogen atmosphere.

around 30 °C, and it became difficult to identify with the increase of POSS content. It is possible that the rigid POSS units lowered the flexibility and mobility of the whole block copolymer, leading to a restricted glass-transition behaviour.

The thermostabilities of the POSS-functionalized LC BCPs were evaluated using TGA under atmospheres of both air and nitrogen, separately (Fig. 4). Obviously, all the LC BCPs exhibit a two-step degradation process under air and a single-step degradation progress under nitrogen. The char yield at 800 °C increased with the increase of POSS content, and the amount of residual char formed under the air atmosphere was significantly higher than that formed under the nitrogen atmosphere, which could be attributed to the silicon dioxide that oxidized from the POSS units. Particularly, the LC BCP with higher POSS content showed a higher 10 wt% decomposition temperature (T_{10}) under both atmospheres. Under the air atmosphere, the initial decomposition temperatures of all the LC BCPs were around 300 °C, indicating that these LC BCPs underwent similar degradation processes, which possibly occurred through the aromatization and dehydrogenation of the alkyl groups. The second degradation process, which occurs at around 470 °C, could be the oxidation of the aromatic rings in the LC units and the further decomposition of the POSS units. Under the nitrogen atmosphere, the LC BCPs with different POSS content showed similar degradation rates after 600 °C. Overall, the TGA results demonstrated that POSS

can substantially enhance the thermostability and the flame retardancy of the LC BCPs.

Temperature range of the LC BCP doped BP

As we all know, the crosslinking density of a polymer in a common PSBP system should be appropriate, because a crosslinking density that is too low will lead to insufficient stabilization,^{58,66} while a crosslinking density that is too high will lead to destruction of the BP structure.⁶⁷ In this POSS-functionalized LC BCP doped BP system, the entanglement of the polymer chains has a similar effect of molecular anchoring on the arrangement of the LCs, and an appropriate crosslinking density (*i.e.* the density of the polymer entangled mesh), which is determined from the length of the polymer chain, should be beneficial for achieving better thermostability. Furthermore, the miscibility of the dopant in the BP is also a crucial factor for stabilizing the BP. Thus, we chose a POSS-functionalized LC BCP with a moderate molecular weight, *i.e.* PHEMAPOSS₄₀-*b*-P6CBMA₁₆₇, denoted POSS-LC-BCP for simplicity, which should contribute to a desired crosslinking density, and its content of mesogenic cyanobiphenyl is higher than 50 wt%, which should improve the miscibility of the whole polymer in the BPLC host, therefore preventing the aggregation of POSS.⁶¹ As shown in Fig. 5a, the BPLC host possesses a narrow BP range of 6.6 °C during cooling, from the phase transition temperature between isotropy and the BP (*i.e.* 87.0 °C) to the phase transition temperature between the BP and the N* phase (*i.e.* 80.4 °C). As a small amount of POSS-LC-BCP was homogeneously mixed into the host system, the optical texture (Fig. 5b) displayed green-coloured platelets with a small size at the temperature close to the upper-end of the BP range, *i.e.* 86.6 °C. The BP domain size gradually increased and was accompanied by a reflection colour shift to dark blue with cooling until the temperature reached 78.2 °C, *i.e.* the phase transition temperature from the BP to the N* phase, which indicated a slight widening of the BP range to 8.4 °C. In general, better BP stabilization and E-O performance can be achieved in a conventional PSBP system containing a higher concentration of polymer (*i.e.* a higher content of photopolymerizable monomers, *e.g.* 15 wt%), as suggested in many prior studies.^{51,53,68} Thus, we attempted to increase the concentration of the LC BCP to 15 wt% in the BPLC host. Surprisingly, a much wider BP range of 44 °C, from 79 °C to 35 °C, was observed, exhibiting a reflection colour change of the platelets from the initial green mixed up with blue to the final blue colour, and was accompanied by the shrinkage of the platelet size with cooling (Fig. 5c). A continuous increase of the POSS-LC-BCP concentration to 20 wt% led to further widening of the BP range from 80 °C to 23 °C, including the typical room temperature range (*i.e.* 25 °C–30 °C), displaying a reflection colour change from cyan to dark blue as well as the diminishing of the platelets upon cooling (Fig. 5d). However, the BP range was not extended further as expected, but narrowed to less than 10 °C when the concentration of POSS-LC-BCP exceeded 20 wt%, on account of the phase separation between the BPLC host and the polymer additive. The phase transition temperatures corresponding to all the aforementioned samples are summarized in Table S1.† The gradual

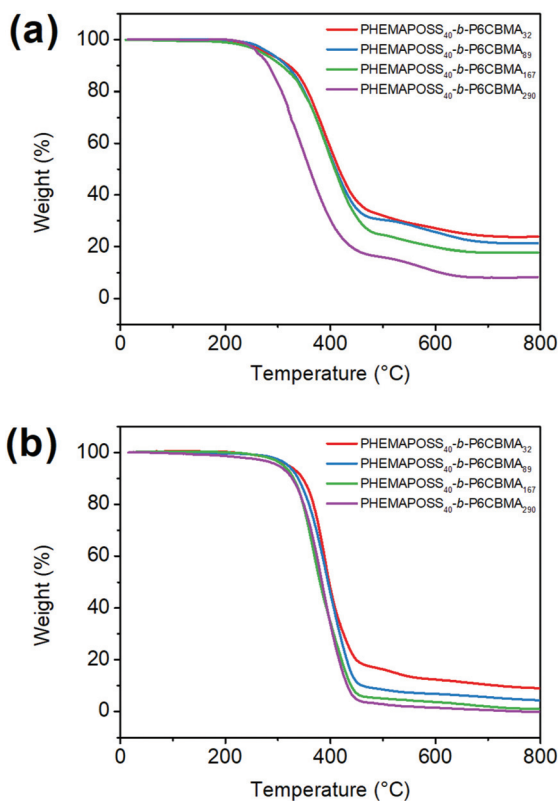


Fig. 4 TGA curves of PHEMAPOSS-*b*-P6CBMA under (a) air and (b) nitrogen atmospheres.

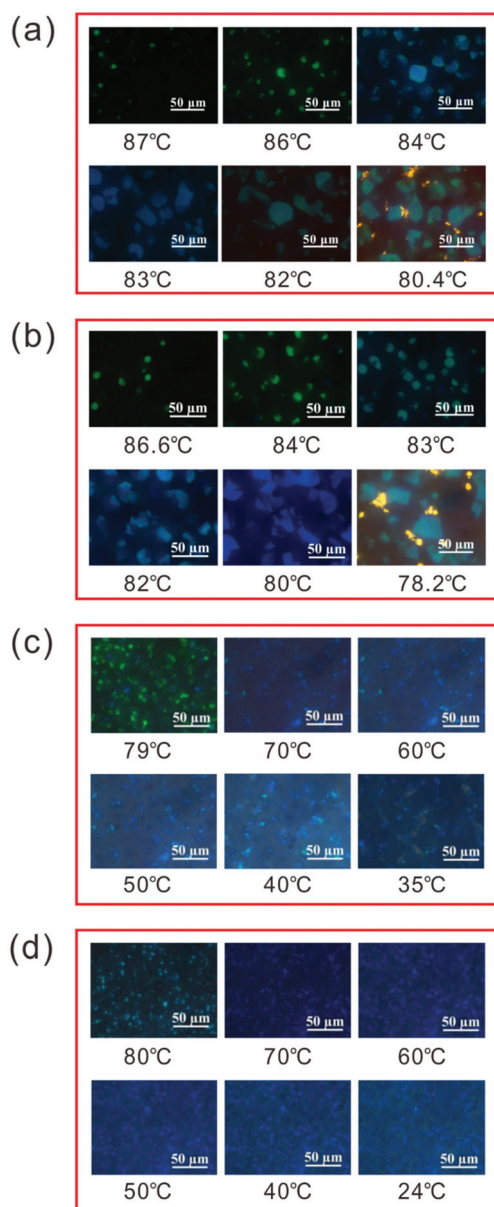


Fig. 5 Optical textures of the BP containing (a) 0 wt%, (b) 5 wt%, (c) 15 wt% and (d) 20 wt% LC BCP observed using the reflection mode of a POM with crossed polarizers. The corresponding temperature is labelled below every panel. Scale bar: 50 μm .

reduction of the phase transition temperature from the isotropic state to the BP ($T_{\text{Iso-BP}}$) indicated good miscibility of POSS-LC-BCP with the BPLC host, and demonstrated that the mesogenic moieties grafted on the polymer chain play a positive role in enhancing the miscibility with the BPLC host. In addition, the BP domain size (*i.e.* platelet size) was found to be reduced significantly with increasing POSS-LC-BCP concentration, due to the shrinkage of the network formed by the polymer chain entanglement of the growing POSS-LC-BCP, which is similar to the effect caused by increasing photocrosslinking density in conventional PSBP systems containing a high monomer content before light exposure. Furthermore, the tex-

tures and the corresponding reflection spectra of the samples containing 20 wt% POSS-LC-BCP were almost invariant (Fig. 5d, Fig. S5d[†]), indicating that enhanced structural stability of the BP has been achieved for the first time in such a convenient manner without subsequent photopolymerization; this is completely distinct from the commonly adopted BP stabilization through photo-induced polymerization, *i.e.* PSBP, and other methods proposed previously.

It was noted that the helical pitch of the BP system was gradually elongated with the doping of POSS-LC-BCP, determined from the red-shift of the central wavelength (λ_c) of the reflection band (Fig. S6[†]). This should have led to a reduction in the stability of the BP. On the contrary, it has been confirmed that the high concentration of POSS-LC-BCP (≤ 20 wt%) facilitated the stabilization of the BP. The reason for such an effect may lie in the anchoring effect of the LC arrangement on the surface of the polymer caused by entanglement of the polymer chains, therefore resulting in the enhancement of the BP stability, however, the POSS induced low interfacial energy between the defect and DTCs in the BP cubic structure also plays a positive role.

E-O Performance

The voltage dependent transmittance of the BPLC containing 20 wt% POSS-LC-BCP exhibited a lower driving voltage of 69 V, which declined sharply for approximately 90 V, compared with that of the conventional PSBP sample; meanwhile the E-O hysteresis for the former was less than half of that for the latter (Fig. 6a). Such exciting improvements of E-O performance probably result from the lower interfacial energy between the defects and DTCs in the former BP sample. To reduce the driving voltage further, the LC host can be changed to a material with higher dielectric constant or the protrusion electrodes can be designed according to the distribution of the electric-field lines. Besides, adopting such polymer doping to enhance the BP cubic structure presented a weak influence on the response behaviour of the BP. The rise and decay times were 130 μs and 300 μs (Table S2[†]), which are comparable to those of the typical BPLC and the PSBP demonstrated herein.

The parameter K – a specific index to reflect the performance of the BP driven by an electric field – of the BP containing 20 wt% POSS-LC-BCP was 1.96 nm V^{-2} , which was conspicuously higher than that of the PSBP, 0.75 nm V^{-2} , as predicted. K is proportional to the birefringence (Δn), the dielectric constant ($\Delta\epsilon$) and the square of the helical pitch (P^2) of a given LC system as expressed in eqn (1),⁵¹

$$K \approx \Delta n \cdot \Delta\epsilon \frac{\epsilon_0 P^2}{k\lambda(2\pi)^2} \quad (1)$$

in which k is the average elastic constant and λ is the wavelength of light. Conspicuous monotonic decreases in Δn and $\Delta\epsilon$ of 0.028 and 9.259, respectively, were observed as the content of POSS-LC-BCP was increased to 20 wt% (Fig. 6b), probably due to the isotropic orientation of the mesogenic moieties in the side chains of the doped polymers. However, the helical pitch was extended for about 20 nm as aforemen-

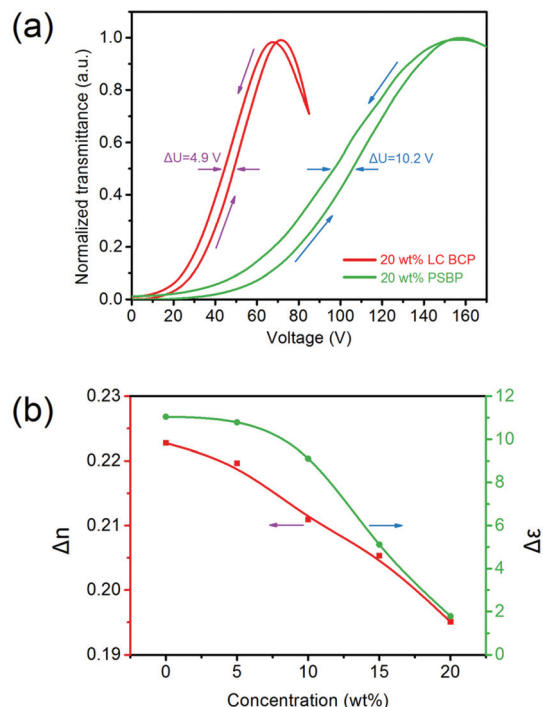


Fig. 6 (a) The VT curves of the different blue phase systems. The PSBP system herein was doped with 4.8 wt% chiral dopant and 20 wt% acrylate-based monomers, then polymerized using UV (365 nm) light at 1 mW cm^{-2} for 30 min. The hysteresis (ΔU) was defined as the voltage-differences at 50% transmittance of the loops (i.e. the width of the loops at 50% transmittance). (b) Δn and $\Delta \epsilon$ of the blue phase systems with different concentrations of LC BCPs.

tioned, and moreover, K is a function of the quadratic term of P , leading to a higher value of K mathematically.

Conclusions

We prepared POSS-functionalized LC BCPs (PHEMAPOSS-*b*-P6CBMA) consisting of a POSS block and a mesogenic cyanobiphenyl block *via* RAFT polymerization to facilitate dope into a BP system, which revealed a new strategy that is distinct from the conventional polymer stabilization strategy used to stabilize the BP. By virtue of the advantages of both the POSS and polymer, we successfully extended the BP range to room temperature and achieved a lower driving voltage, lower hysteresis and higher K when increasing the concentration of the LC BCP to 20 wt%, displaying significant improvements compared with the common PSBP sample. Such an ingenious BP stabilization gives rise to another stable BP helical superstructure candidate for facilitating practical application not only in large size BP displays but in other applications beyond this.

Conflicts of interest

There are no conflicts to declare.

Acknowledgements

This work was financially supported by the National Natural Science Foundation of China (No. 21574039, 61575063, 61435008, 61775212 and 51173044), Shanghai Rising-Star Program (No. 17QA1401100), the Fundamental Research Funds for the Central Universities (222201817002), and State Key Laboratory of Applied Optics (No. M200-D-1716).

References

- 1 Y. Y. Mao, Q. Zhao, J. C. Wu, T. T. Pan, B. P. Zhou and Y. Q. Tian, *J. Mater. Chem. C*, 2017, **5**, 11395–11402.
- 2 X. F. Yu, Y. W. Li, X. H. Dong, K. Yue, Z. W. Lin, X. Y. Feng, M. J. Huang, W. B. Zhang and S. Z. D. Cheng, *J. Polym. Sci., Part B: Polym. Phys.*, 2014, **52**, 1309–1325.
- 3 W. A. Zhang and A. H. E. Müller, *Prog. Polym. Sci.*, 2013, **38**, 1121–1162.
- 4 Y. Xu, H. Xu, X. Jiang and J. Yin, *Adv. Funct. Mater.*, 2014, **24**, 1679–1686.
- 5 H. Hou, Y. Gan, J. Yin and X. Jiang, *Adv. Mater. Interfaces*, 2014, **1**, 1400385.
- 6 Z. Zhang, P. Zhang, Y. Wang and W. Zhang, *Polym. Chem.*, 2016, **7**, 3950–3976.
- 7 Y. S. Ye, W. C. Shen, C. Y. Tseng, J. Rick, Y. J. Huang, F. C. Chang and B. J. Hwang, *Chem. Commun.*, 2011, **47**, 10656–10658.
- 8 K. Yue, C. Liu, K. Guo, X. F. Yu, M. J. Huang, Y. W. Li, C. Wesdemiotis, S. Z. D. Cheng and W. B. Zhang, *Macromolecules*, 2012, **45**, 8126–8134.
- 9 Y. J. Pu, L. G. Zhang, H. Zheng, B. He and Z. W. Gu, *Polym. Chem.*, 2014, **5**, 463–470.
- 10 Y. Y. Yang, X. Wang, Y. Hu, H. Hu, D. C. Wu and F. J. Xu, *ACS Appl. Mater. Interfaces*, 2014, **6**, 1044–1052.
- 11 X. Fan, Z. Wang and C. He, *J. Mater. Chem. B*, 2015, **3**, 4715–4722.
- 12 W. A. Zhang, B. Fang, A. Walther and A. H. E. Müller, *Macromolecules*, 2009, **42**, 2563–2569.
- 13 X. Yu, S. Zhong, X. Li, Y. Tu, S. Yang, R. M. Van Horn, C. Ni, D. J. Pochan, R. P. Quirk, C. Wesdemiotis, W. B. Zhang and S. Z. Cheng, *J. Am. Chem. Soc.*, 2010, **132**, 16741–16744.
- 14 W. Zhang and A. H. E. Müller, *Macromolecules*, 2010, **43**, 3148–3152.
- 15 B. Ni, M. Huang, Z. Chen, Y. Chen, C. H. Hsu, Y. Li, D. Pochan, W. B. Zhang, S. Z. Cheng and X. H. Dong, *J. Am. Chem. Soc.*, 2015, **137**, 1392–1395.
- 16 M. Huang, C. H. Hsu, J. Wang, S. Mei, X. Dong, Y. Li, M. Li, H. Liu, W. Zhang, T. Aida, W. B. Zhang, K. Yue and S. Z. Cheng, *Science*, 2015, **348**, 424–428.
- 17 H. Zhang, S. Ma, Y. Yao, Y. Li, Y. Li, J. Ou, M. Ye and Y. Wei, *J. Chromatogr. A*, 2017, **1524**, 135–142.
- 18 Y. Pu, S. Chang, H. Yuan, G. Wang, B. He and Z. Gu, *Biomaterials*, 2013, **34**, 3658–3666.
- 19 D. Li, Y. Niu, Y. Yang, X. Wang, F. Yang, H. Shen and D. Wu, *Chem. Commun.*, 2015, **51**, 8296–8299.

- 20 G. C. Yuan, X. Wang, D. C. Wu and B. Hammouda, *Polymer*, 2016, **100**, 119–125.
- 21 Z. H. Zhang, L. Z. Hong, J. X. Li, F. Liu, H. B. Cai, Y. Gao and W. A. Zhang, *RSC Adv.*, 2015, **5**, 21580–21587.
- 22 Z. H. Zhang, L. Z. Hong, Y. Gao and W. A. Zhang, *Polym. Chem.*, 2014, **5**, 4534–4541.
- 23 M. G. Mohamed, K. C. Hsu, J. L. Hong and S. W. Kuo, *Polym. Chem.*, 2016, **7**, 135–145.
- 24 Z. Zhang, Y. Xue, P. Zhang, A. H. E. Müller and W. Zhang, *Macromolecules*, 2016, **49**, 8440–8448.
- 25 T. Hirai, M. Leolukman, C. C. Liu, E. Han, Y. J. Kim, Y. Ishida, T. Hayakawa, M. A. Kakimoto, P. F. Nealey and P. Gopalan, *Adv. Mater.*, 2009, **21**, 4334–4338.
- 26 B. H. Tan, H. Hussain and C. B. He, *Macromolecules*, 2011, **44**, 622–631.
- 27 C. J. Yang, Y. M. Deng, B. R. Zeng, C. H. Yuan, M. Chen, W. A. Luo, J. Liu, Y. T. Xu and L. Z. Dai, *J. Polym. Sci., Part A: Polym. Chem.*, 2012, **50**, 4300–4310.
- 28 T. Hirai, M. Leolukman, S. Jin, R. Goseki, Y. Ishida, M.-a. Kakimoto, T. Hayakawa, M. Ree and P. Gopalan, *Macromolecules*, 2009, **42**, 8835–8843.
- 29 B. Ahn, T. Hirai, S. Jin, Y. Rho, K.-W. Kim, M.-a. Kakimoto, P. Gopalan, T. Hayakawa and M. Ree, *Macromolecules*, 2010, **43**, 10568–10581.
- 30 Y. Tada, H. Yoshida, Y. Ishida, T. Hirai, J. K. Bosworth, E. Dobisz, R. Ruiz, M. Takenaka, T. Hayakawa and H. Hasegawa, *Macromolecules*, 2012, **45**, 292–304.
- 31 R. Nakatani, H. Takano, A. Chandra, Y. Yoshimura, L. Wang, Y. Suzuki, Y. Tanaka, R. Maeda, N. Kihara, S. Minegishi, K. Miyagi, Y. Kasahara, H. Sato, Y. Seino, T. Azuma, H. Yokoyama, C. K. Ober and T. Hayakawa, *ACS Appl. Mater. Interfaces*, 2017, **9**, 31266–31278.
- 32 F. Zhou, K. H. Gu, Z. Y. Zhang, M. Y. Zhang, S. Zhou, Z. Shen and X. H. Fan, *Angew. Chem., Int. Ed.*, 2016, **55**, 15007–15011.
- 33 P.-F. Cao, Z. Wojnarowska, T. Hong, B. Carroll, B. Li, H. Feng, L. Parsons, W. Wang, B. S. Lokitz, S. Cheng, V. Bocharova, A. P. Sokolov and T. Saito, *Polymer*, 2017, **124**, 117–127.
- 34 C. Zhang, D. Wang, J. He, M. Liu, G.-H. Hu and Z.-M. Dang, *Polym. Chem.*, 2014, **5**, 2513.
- 35 Y.-D. Zhang, J. Ping, Q.-W. Wu, H.-B. Pan, X.-H. Fan, Z. Shen and Q.-F. Zhou, *Polym. Chem.*, 2017, **8**, 1689–1698.
- 36 K. Yuan, L. Chen and Y. Chen, *J. Mater. Chem. C*, 2014, **2**, 3835–3845.
- 37 A. Nunns, J. Gwyther and I. Manners, *Polymer*, 2013, **54**, 1269–1284.
- 38 L. Gao, Z. Shen, X. Fan and Q. Zhou, *Polym. Chem.*, 2012, **3**, 1947.
- 39 K. K. Tenneti, X. Chen, C. Y. Li, X. Wan, X. Fan, Q.-F. Zhou, L. Rong and B. S. Hsiao, *Soft Matter*, 2008, **4**, 458–461.
- 40 J. He, L. Tremblay, S. Lacelle and Y. Zhao, *Polym. Chem.*, 2014, **5**, 5403–5411.
- 41 S. Fu and Y. Zhao, *Macromolecules*, 2015, **48**, 5088–5098.
- 42 Z. Shi, D. Chen, H. Lu, B. Wu, J. Ma, R. Cheng, J. Fang and X. Chen, *Soft Matter*, 2012, **8**, 6174.
- 43 H. Yu, T. Kobayashi and H. Yang, *Adv. Mater.*, 2011, **23**, 3337–3344.
- 44 W. Fan, X. Tong, G. Li and Y. Zhao, *Polym. Chem.*, 2017, **8**, 3523–3529.
- 45 T. Wang, X. Li, Z. Dong, S. Huang and H. Yu, *ACS Appl. Mater. Interfaces*, 2017, **9**, 24864–24872.
- 46 H. Kikuchi, *Struct. Bonding*, 2008, **128**, 99–117.
- 47 Z.-g. Z. Zhi-gang Zheng, W. H. Wei Hu, G. Z. Ge Zhu, M. S. Mu Sun, D. S. Dong Shen and Y.-q. L. Yan-qing Lu, *Chin. Opt. Lett.*, 2013, **11**, 011601–011605.
- 48 K. M. Chen, S. Gauza, H. Xianyu and S. T. Wu, *J. Disp. Technol.*, 2010, **6**, 49–51.
- 49 J. Guo, Y. Shi, X. Han, O. Jin, J. Wei and H. Yang, *J. Mater. Chem. C*, 2013, **1**, 947–957.
- 50 K. Kishikawa, H. Itoh, S. Akiyama, T. Kobayashi and S. Kohmoto, *J. Mater. Chem.*, 2012, **22**, 8484.
- 51 L. Wang, W. He, Q. Wang, M. Yu, X. Xiao, Y. Zhang, M. Ellahi, D. Zhao, H. Yang and L. Guo, *J. Mater. Chem. C*, 2013, **1**, 6526.
- 52 W.-Q. Yang, G.-Q. Cai, Z. Liu, X.-Q. Wang, W. Feng, Y. Feng, D. Shen and Z.-g. Zheng, *J. Mater. Chem. C*, 2017, **5**, 690–696.
- 53 H. Kikuchi, S. Izena, H. Higuchi, Y. Okumura and K. Higashiguchi, *Soft Matter*, 2015, **11**, 4572–4575.
- 54 I. Dierking, W. Blenkhorn, E. Credland, W. Drake, R. Kociuruba, B. Kayser and T. Michael, *Soft Matter*, 2012, **8**, 4355.
- 55 I. Dierking, *Polym. Chem.*, 2010, **1**, 1153.
- 56 W. L. He, W. K. Zhang, H. Xu, L. H. Li, Z. Yang, H. Cao, D. Wang, Z. G. Zheng and H. Yang, *Phys. Chem. Chem. Phys.*, 2016, **18**, 29028–29032.
- 57 H. Ocak, B. Bilgin-Eran, M. Prehm, S. Schymura, J. P. F. Lagerwall and C. Tschierske, *Soft Matter*, 2011, **7**, 8266.
- 58 H. Kikuchi, M. Yokota, Y. Hisakado, H. Yang and T. Kajiyama, *Nat. Mater.*, 2002, **1**, 64–68.
- 59 Y. Li, S. Huang, P. Zhou, S. Liu, J. Lu, X. Li and Y. Su, *Adv. Mater. Technol.*, 2016, **1**, 1600102.
- 60 Y. Chen and S.-T. Wu, *J. Appl. Polym. Sci.*, 2014, **131**, 40556.
- 61 D.-Y. Kim, S. Kim, S.-A. Lee, Y.-E. Choi, W.-J. Yoon, S.-W. Kuo, C.-H. Hsu, M. Huang, S. H. Lee and K.-U. Jeong, *J. Phys. Chem. C*, 2014, **118**, 6300–6306.
- 62 E.-H. Kim, S.-W. Myoung, W.-R. Lee and Y.-G. Jung, *J. Korean Phys. Soc.*, 2009, **54**, 1180–1186.
- 63 E. Kemiklioglu, J. Y. Hwang and L. C. Chien, *Phys. Rev. E: Stat. Phys., Plasmas, Fluids, Relat. Interdiscip. Top.*, 2014, **89**, 6.
- 64 L. Z. Hong, Z. H. Zhang, Y. Zhang and W. A. Zhang, *J. Polym. Sci., Part A: Polym. Chem.*, 2014, **52**, 2669–2683.
- 65 Y. Hisakado, H. Kikuchi, T. Nagamura and T. Kajiyama, *Adv. Mater.*, 2005, **17**, 96–98.
- 66 X. Li, W. Q. Yang, C. L. Yuan, Z. Liu, K. Zhou, X. Q. Wang, D. Shen and Z. G. Zheng, *Sci. Rep.*, 2017, **7**, 10383.
- 67 N. Kasch, I. Dierking and M. Turner, *Soft Matter*, 2013, **9**, 4789.
- 68 D.-C. Hu, W.-H. Li, X.-W. Chen, X.-L. Ma, Y.-J. Lee and J.-G. Lu, *J. Soc. Inf. Disp.*, 2016, **24**, 593–599.